Anal Bioanal Chem (2010) 398:2341–2349
DOI 10.1007/s00216-010-4027-7

REVIEW

Electrochemical impedance spectroscopy in label-free biosensor applications: multivariate data analysis for an objective interpretation

Britta Lindholm-Sethson · Josefina Nyström · Martin Malmsten · Lovisa Ringstad · Andrew Nelson · Paul Geladi

Received: 27 April 2010 / Revised: 24 June 2010 / Accepted: 12 July 2010 / Published online: 31 July 2010

Abstract Electrochemical impedance spectroscopy plays an important role in biosensor science thanks to the possibility of finding specific information from processes with different kinetics at a chosen electrode potential in one experiment. In this paper we briefly discuss label-free impedimetric biosensors described in the literature. A novel method for neutral interpretation of impedance data is presented that includes complex number chemometrics. Three examples are given based on impedance measurements on synthetic biomembranes, in this case a lipid monolayer deposited on a mercury electrode. The interaction of various compounds with the monomolecular lipid layer is illustrated with the following: (1) different concentrations of magainin (Geladi et al. in *Proc. Int. Fed. Med. Biomed. Eng.* 9:219–220, 2005); (2) different derivatives of gramicidin A (Lindholm-Sethson et al. in *Langmuir* 24:5029–5032, 2007), and (3) an antimicrobial peptide (Ringstad et al. in *Langmuir* 24:208–216, 2008).

Keywords Impedance · Biosensor · Complex number chemometrics

Published in the special issue on *Focus on Bioanalysis* with Guest Editors Antje J. Baeumner, Günter Gauglitz, and Frieder W. Scheller.

B. Lindholm-Sethson (✉) · J. Nyström
Department of Chemistry, Umeå University,
901 87 Umeå, Sweden
e-mail: britta.sethson@chem.umu.se

M. Malmsten · L. Ringstad
Department of Pharmacy, Uppsala University,
751 23 Uppsala, Sweden

A. Nelson
Centre for Molecular Nanoscience, School of Chemistry,
University of Leeds,
Leeds LS2 9JT, UK

P. Geladi
Unit of Biomass Technology and Chemistry, SLU,
90183 Umeå, Sweden

Introduction

In general

Electrochemical biosensors form one particular type of sensor where the response from a biological recognition element is transduced by means of an electrochemical method, such as amperometry, voltammetry, or impedance. The present paper relates to impedance biosensors and the possibility of the development of label-free detection. Therefore, enzyme biosensors and nanoparticle-labeled systems will not be mentioned, although their importance is recognized.

Impedance spectroscopy is a powerful technique because it allows the probing of processes with various time constants in the electrode/electrolyte interface in a single experiment. The possibility to develop cheap, robust, and small instrumentation that allows real-time analysis is shared with other electroanalytical techniques. Because different interactions have different time constants, multiplexing is possible as is demonstrated by the simultaneous detection of doxorubicin and some of its various metabolites with electrochemical techniques [1]. Future application areas for the impedimetric sensor include point-of-care diagnostics [2–4], determination of freshwater toxins [5], explosives such as 2,4,6-trinitrotoluene, i.e., TNT [6], environmental science, pharmaceutical and food industries, and clinical chemistry [7].

The impedance sensors are often partitioned in two categories, faradaic or nonfaradaic. With *faradaic detection* a redox probe is added to the solution and the heterogeneous electron-transfer resistance, R_{ct}, is monitored. A charged surface presents either an attractive or a repulsive force on ions near the electrode, which can significantly affect R_{ct}. The surface charge depends on pH, temperature, and other factors, such as calcium binding to negatively charged lipid head groups in a lipid layer. R_{ct} of the probe is also affected by pore formation or changes in film thickness on binding of a target to the probe in an immunosensor or a change in the molecular conformation thickness [8].

A *nonfaradaic sensor* generally relies on an equivalent circuit where the assumed processes are mimicked by ideal circuit elements with ordinary lumped-constant properties. A change in capacitance is often used for determination of the concentration of an analyte in solution. A common equivalent circuit consists of three capacitors in series; these are the self-assembled membrane itself, the probe layer, and the double layer.

In reality, a distribution of relaxation times is prevalent and therefore the ideal elements are substituted with distributed ones, such as constant phase elements and/or infinite transmission lines. The dipoles in the head group of a lipid layer or a self-assembled monolayer at an electrode surface affect the dielectric constant of the layer. Ion pairing with ions in solution alters the relaxation times and also one or more of the capacitances in the interface [9].

Instead of the equivalent circuits, an exact mathematical model can be developed based on a plausible physical theory for the processes in the interfacial region. In biomimetic systems the comparison with dielectric relaxation theory is obvious and is also pursued in some cases to find mathematical models [10]. In a realistic model the ideal Debye circuit should be exchanged for the more generalized Cole–Cole model to allow for a dispersion of relaxation times (see also "Electrochemical impedance spectroscopy in the light of dielectric relaxation theory").

In both cases, i.e., with equivalent circuit modeling or with a predicted $Z_t(\omega)$ from the mathematical model, complex nonlinear least-squares fitting is preferred and also used to find precise information on the system. The authors propose the usage of complex number multivariate data analysis for noise reduction before selecting a model.

The present situation

The most successful electrochemical sensor so far is the amperometric or coulometric glucose sensor [11]. One of the first impedance biosensors was reported in 1988 and concerned the detection of acetylcholine [12]. The acetylcholine receptor protein was incorporated into liposomes and fused on the surface of an interdigitated sensor surface, and the capacitance increased rapidly when acetylcholine was added to the solution. Below we give some examples from the literature of various impedimetric label-free biosensors without the intention to provide a complete coverage. More exhaustive reviews can be found elsewhere [13, 14].

An *affinity sensor* detects the target molecule when it binds to an immobilized probe as a change in surface impedance. Here the immobilized probe brings selectivity to the device. The sensing surface can be placed in the gap between electrodes in an interdigited array or directly on top of the electrode surface. In the former case, the gap is modified for affinity binding and impedance measurements can detect resistive or capacitive changes as demonstrated by van Gerwen et al. [15] and by Laureyn et al [16]. In the latter case, the impedimetric immunosensor is based on the interaction between an antibody and an electrode that is functionalized with an antigen. The antigen–antibody complex that is formed in the interface affects both the capacitance and the charge-transfer resistance in the interface. A nonfaradaic detection was accomplished by Rickert et al. [17] where a change in the absolute impedance value was used to detect the foot-and-mouth disease virus antibody with a synthetic polypeptide antigen. In this case the kinetics of the antigen–antibody binding was also investigated. A faradaic impedance sensor was evaluated in [18]. However, the surface layer contained pinholes that the redox probe could penetrate and thus the change in charge-transfer resistance was only minor. In the same paper it was also demonstrated how the expected results could be obtained with a nonfaradaic setup.

A *molecular imprinting (MIP) sensor* is produced by fabrication of artificial receptors by, for instance, polymerization around a molecule. When the molecule is removed, a hole is created that exactly matches the shape and size of the molecule. This hole constitutes a specific recognition element for the sensor. A MIP sensor for detection of l-nicotine in the presence of l-cotinine was demonstrated [19]. The detection was based on changes in capacitance and a detection limit of 1 nM was obtained Although l-cotinine only differs by one oxygen atom from l-nicotine a surprisingly high selectivity for l-cotinine was obtained. The MIP-based impedimetric sensor was also useful for detection of other small molecules.

DNA sensors can be produced by modification of an electrode with an oligonucleotide and the formation of nucleic acid–DNA complexes can give quantitative information on the DNA analyte in the test solution. This was demonstrated by Wang et al. [20], who reported a detection limit of 4×10^{-9} M for the human immunodeficiency virus type 1 U5 long tandem repeat segment following a 30-min DNA hybridization. Moreover, Patolosky et al. [21] reported on a biosensor consisting of a thiol-thymine-tagged oligonucleotide that is immobilized on a gold

electrode. A reaction between the modified electrode and a biotinylated oligonucleotide that is complexed with DNA makes possible a quantitative analysis of the concentration of the target DNA. Ultrasensitive impedimetric sensors for detection of viral DNA were reported by Patolosky et al. [22] with detection limits in the femtomolar range. All the DNA sensors mentioned above rely on the faradaic detection of alterations in the interface.

Aptamers are also called "synthetic antibodies" and are produced through an in vitro selection process. A specific monomer sequence is identified that tightly binds the target. These aptamers are promising candidates as substitutes for proteins or antibodies in biosensors especially since they allow label-free and reagentless detection. The possibility for easy production and exploitation of well-understood tethering chemistry and maybe also the possibility to avoid extensive cross-reactions is certainly attractive. Three research groups presented the method of aptamer production independently of each other [23–25].

Thiol-labeled aptamers were immobilized onto gold nanoparticles and used for electrochemical detection of a platelet-derived growth factor [26] with a redox probe. A detection limit of 0.01 pM was reported. Polsky et al. [27] reported on aptamer modification of platinum nanoparticles, where the sensitivity of the method for detection of thrombin was improved by catalysis of the reduction of H_2O_2 at platinum nanoparticle labels, giving an ultrasensitive detection of 10 fM. Furthermore, recently Sharon et al. [28] demonstrated self-organization of aptamer fragments on gold nanoparticles for impedimetric analysis of cocaine based on aptamer–substrate complex formation. Reagentless nonfaradaic impedimetric aptasensors have also been reported [29].

Self-assembled monolayers with attached probes constitute well-developed sensor systems. One interesting example is from Miura et al. [30], where a well-packed monolayer of helical peptides with a crown ether unit was tethered to planar gold electrodes for cation recognition. Impedance spectra were measured in the presence of 0.1 M $Ru(NH_3)_6^{2+/3+}$ and K^+, Cs^+, Na^+, and Li^+ ions. An ordinary Randles circuit was used for data fitting and the cation–crown ether complexation could be observed as a significant increase in the membrane capacitance, except for Li^+ ions. In a different approach at our laboratory with multivariate analysis of impedance data, cation recognition could be accomplished at a single lipid layer without faradaic detection or attached probes [31].

Interdigited array sensors for bacterial cell detection monitor changes in the impedance data owing to specific biorecognition elements, such as nonspecific adsorption of cells, detection of metabolites, or based on the charge of the cell. Both nonfaradaic analysis and faradaic detection have been employed [32].

Present methods for impedance data analysis necessitate a primary assumption regarding the system. Subsequent data analysis through data fitting immediately gives data reduction as a consequence. Therefore, we have initiated the development of chemometric methods for the analysis of impedance data. This provides the possibility for an unbiased first analysis of the data that can lead to either a multivariate regression in electroanalysis or an indication on a plausible equivalent circuit or physical model. The purpose of this paper is to demonstrate this method with some examples from our recent work.

Electrochemical impedance spectroscopy in the light of dielectric relaxation theory

Many scientific papers concern the characterization of a supported lipid membrane at an electrode surface by electrochemical impedance spectroscopy. Sometimes an electroactive probe is used to enhance the signal and in these cases the heterogeneous rate constant is used as a marker for some biological process in the interface. In other cases a nonfaradaic response is obtained. This was described briefly in the previous section. In both cases an extensive data fitting to various sophisticated models is frequently employed. Surprisingly, dielectric relaxation theory has not been employed to a larger extent to guide of the choice of models. Some of these thoughts are introduced in this paper.

Investigations of dielectric properties of tissues and other biological systems have been of interest to biophysicists for more than a century [33, 34]. In particular, it is worth mentioning one of the first estimations of the molecular thickness of cell membranes, which was performed by Fricke [35] with dielectric relaxation studies in cell suspensions.

Briefly, the measurements involve the injection of an alternating current into the tissue and measurement of the resulting alternating voltage, and the absolute impedance, $|Z|$, and phase shift, θ, can be easily calculated. In electrochemical impedance spectroscopy the opposite is often the case, i.e., an alternating voltage is imposed on the electrode and the resulting alternating current is measured. In the latter case, control of the electrode potential is often essential. This makes it impossible to reach very high frequencies because of limitations of the potentiostats.

Nevertheless, in both cases the impedance data are frequently displayed in the complex impedance plane. i.e., $Z^* = Z' + jZ''$, where the real part is $Z' = |Z^*| \cos\theta$ and the imaginary part is $Z'' = |Z^*| \sin\theta$; j^2=-1.

To get a physiological understanding of the dielectric relaxation data, a transformation to parameters such as permittivity and conductance is often valuable. This is

easily accomplished through the relationship $C^* = 1/j\omega Z^*$, where ω is the angular frequency. The complex capacitance, C^*, is closely related to the complex relative permittivity, $\varepsilon^* = \varepsilon' - j\varepsilon''$, through $C^* = \varepsilon^* \varepsilon_0 A/d$. Here, an idealized parallel-plate capacitor is considered, where A is the plate area and d is the separation; ε_0 is the permittivity of free space.

The real part of the complex permittivity, ε', can be identified as the so-called dielectric constant, which is essentially constant at low frequencies. Here we refer to ε' as permittivity, which reflects the polarizability of "localized" charge distributions, such as electrical double layers at membrane/electrode surfaces or around solvated macromolecules.

The imaginary part of the complex permittivity is known as the dielectric loss, which is associated with movement of polarizable charges in phase with the electric field. The dielectric loss is related to the frequency-dependent conductivity, $\sigma(\omega)$:

$$\varepsilon'' = \sigma(\omega)/\omega\varepsilon_0 = [\sigma_0 + \sigma_d(\omega)]/\omega\varepsilon_0, \quad (1)$$

where σ_0 is the steady-state conductivity arising primarily from mobile ions and $\sigma_d(\omega)$ is the frequency-dependent conductivity stemming from dielectric relaxation.

The essential model for dielectric relaxation is the Debye dispersion relation, where only a single relaxation is considered [36]:

$$\varepsilon^* - \varepsilon_\infty = \frac{\varepsilon_s - \varepsilon_\infty}{[1 + (j\omega\tau_o)]} \quad (2)$$

Here ε_s is the low-frequency permittivity, where "s" stands for *static*. ε_∞ is a frequency-independent permittivity at high frequencies well above the single Debye relaxation. In Fig. 1a ($\alpha = 0$) ε' is plotted against ε'' for the Debye model and the result is a semicircle in the complex permittivity plane. At low frequencies the intersection with the real axis is at 1 and at high frequencies it is at 0. At the maximum of the semicircle, i.e., at the dielectric loss peak, the transition frequency $\omega_o = \tau^{-1}$ is found and the corresponding characteristic frequency, f_c, is $\omega_o/2\pi$.

The Debye equation assumes a single relaxation frequency, something that is rarely found. The Debye peak is often broadened over its theoretical half-width, which indicates a distribution of relaxation times. One of the most widely used distributions is the Cole–Cole model giving depressed semicircular arcs in the complex permittivity plane. This is described by the Cole–Cole equation [36]:

$$\varepsilon^* - \varepsilon_\infty = \frac{\varepsilon_s - \varepsilon_\infty}{\left[1 + (j\omega\tau_0)^{1-\alpha}\right]} \quad (3)$$

In Fig. 1a the Cole–Cole diagram is shown for some values of α, and in Fig. 1b the dielectric loss is shown for some values of α as a function of frequency. The dielectric loss peak reaches its maximum at τ_0. Note that in the equations above only one type of relaxation is assumed, either a single relaxation or a distribution of relaxations. Normally, there is more than one type of relaxation.

The dielectric dispersion of tissues has been investigated in a wide frequency range, i.e., 0.1–10^{11} Hz, and it is found that living tissue is not characterized by a few single time constant systems but rather by a distribution of relaxation times. Generally, a monotonic decrease in permittivity and a monotonic increase in conductivity with frequency is observed, where three major dispersion regions are often distinguishable, the so-called α, β, and γ dispersions (see Fig. 3.14 in [37]).

In the central part of these dispersion regions the permittivity decreases rapidly, the conductivity increases correspondingly, and the dielectric loss is expected to peak. Between the dispersion regions the conductivity and permittivity reach plateau values and the dielectric loss term tends toward zero. The position of the loss peak provides useful information on the time constant of the polarization process responsible for the particular relaxation. This was demonstrated, for instance, in an investigation of apical membrane of frog skin with dielectric spectroscopy in the α-dispersion region (0.1 Hz to 5.5 kHz). The authors found several populations of relaxation processes centered at four different frequencies, where the process around the lowest frequency, 30 Hz, seemed to be related to sodium transport [38].

The impedance measurements that are reported here were recorded in the frequency regime between 0.1 and 65 kHz. This could be referred to as the α- and β-dispersion region. The β dispersion occurs at the high-frequency end of this spectrum and is primarily related to capacitive charging of the lipid layer. This is analogous to the charging of the cell membrane in a cell suspension via a Maxwell–Wagner effect. The time constant for the relaxation process at the electrode surface is dependent on the solution resistance and the capacitance in the lipid head group region.

The α dispersion occurs at lower frequencies and the major contribution in a cell suspension is due to ion movement tangentially to the cell surface. This can obviously not be observed at a supported lipid layer residing on an electrode surface. The electric field is perpendicular to the electrode surface and therefore this type of relaxation is excluded. This enables observation of other low-frequency processes that otherwise are blurred by the dominating contribution from the tangential movement of ions or the diffusion of lipids or proteins in the cell envelope. These are, for instance, access impedance from the sarcotubular system, [39, 40] field-induced gating of transmembrane ion transfer [41], and rotations of proteins [42].

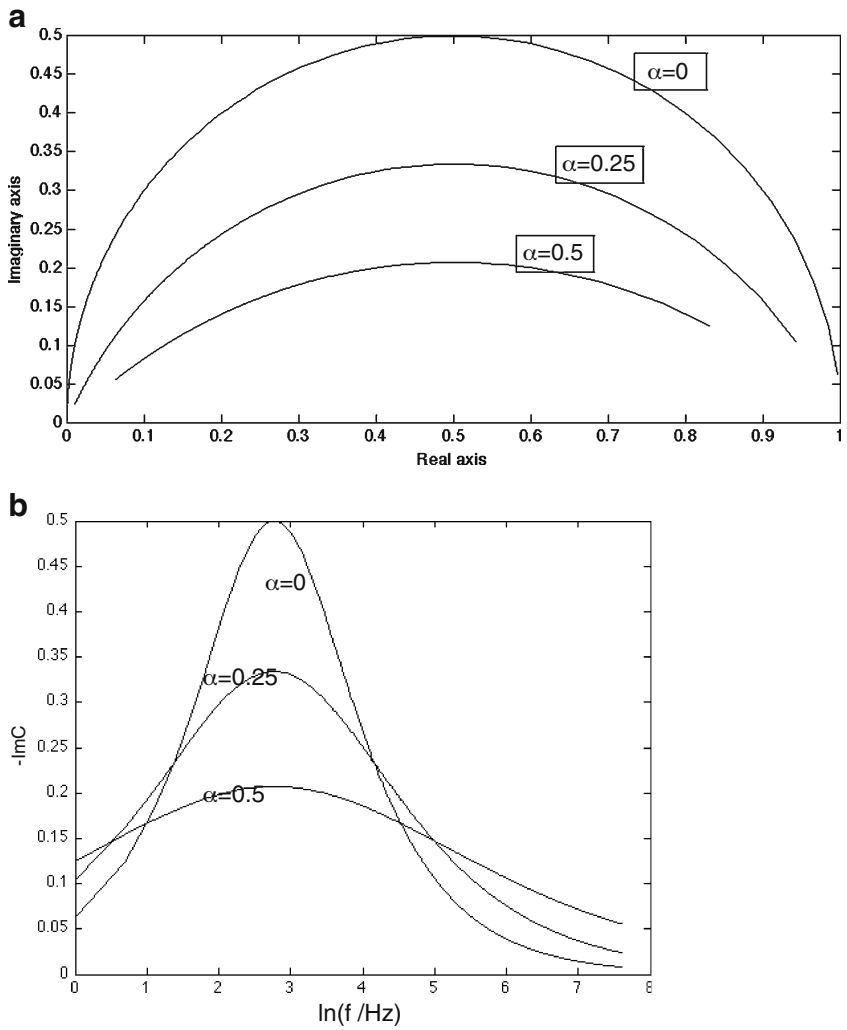

Fig. 1 **a** The generic Debye (α=0) and Cole–Cole (α=0.25, α=0.5) functions for τ_0=0.01 and frequencies 1–2,000 Hz. **b** The imaginary part of Eq. 2 against the logarithm of the frequency for Debye (α=0) and Cole–Cole (α=0.25, α=0.5) models (f_c=16 Hz)

Complex number chemometrics

Theory

Here we briefly describe a method that was first presented in [43]. Multifrequency impedance data are best studied by taking all frequencies into account at once and not by studying the response at each frequency separately. Principal component analysis (PCA) and singular value decomposition (SVD) are methods that are used very often to simplify multivariate data and at the same time to study the structure in the data. The SVD equation is

$$\mathbf{Z} = \mathbf{U}_r \mathbf{S}_r \mathbf{V}_r^{\mathrm{H}} + \mathbf{E}_r, \tag{4}$$

where $\mathbf{Z}$ is a matrix of complex numbers, properly pretreated and/or transformed, $\mathbf{E}_r$ is a matrix of residuals, noise, or irrelevant data, H is a Hermitian (complex conjugate transpose), $\mathbf{U}_r$ is a unitary matrix $\left(\mathbf{U}_r^{\mathrm{H}}\mathbf{U}_r = \mathbf{I}\right)$ with complex score vectors as columns for r components, $\mathbf{V}_r$ is a unitary matrix $\left(\mathbf{V}_r^{\mathrm{H}}\mathbf{V}_r = \mathbf{I}\right)$ with complex loading values as columns for r components, and $\mathbf{S}_r$ is a diagonal matrix with the real singular values on the diagonal for r components.

With only real numbers, unitary matrices become orthonormal and the Hermitian becomes a transpose.

$\mathbf{E}_r$ can be made a matrix of zeros if needed, but usually only components that have interpretable systematic information are used. This leaves the noise components in $\mathbf{E}_r$. The data as obtained from the electrochemical experiment may have 50 real and 50 imaginary variables. It is possible to consider these as 100 separate variables, but it is equally possible to leave them in the complex number form. As preprocessing, the data may be converted into complex capacitance form $\left(C^* = 1/\mathrm{j}\omega Z^*\right)$. It is also possible to carry out mean-centering and scaling as explained in [43].

The vectors in $\mathbf{U}_r$ and $\mathbf{V}_r$ are complex number vectors and can be plotted as Argand diagrams. It was shown earlier [43] that Argand diagrams for one component at a

time may be as useful as scatter plots of two components for real-value PCA.

An important diagnostic is the percentage of the total sum of squares explained. It is assumed that a high proportion of the total sum of squares is explained by the model and that the residual sum of squares is appropriately small. The squared diagonal values in $\mathbf{S}_r$ can also be used to show how much of the total sum of squares each component explains. Depending on the expected noise, this can be an excellent stopping criterion. For a two-component model this would give

$$\mathrm{SS}(\mathbf{Z}) = \mathrm{SS}(\mathbf{s}_1) + \mathrm{SS}(\mathbf{s}_2) + \mathrm{SS}(\mathbf{E}_r), \quad (5)$$

where $\mathrm{SS}(\mathbf{s}_1)$ is the first component sum of squares and $\mathrm{SS}(\mathbf{s}_2)$ is the second component sum of squares, where $\mathbf{s}_1$ and $\mathbf{s}_2$ are diagonal elements of $\mathbf{S}$.

Applications

Three examples will be discussed to demonstrate the usage of complex numbers from impedance spectroscopy using PCA/SVD. The authors are aware of that data sets are small and therefore no calibration models were made. Two of them have already been published [43] and the last example constitutes a new analysis with a data set from [44]. All examples concern the interaction of polypeptides with a monomolecular layer of dioleyl phosphatidylcholine (DOPC) on a mercury drop. Impedance measurements were performed at 50 frequencies logarithmically distributed between 100 mHz and 65,000 Hz with an amplitude of 5 mV rms and at a potential of -400 mV versus 3.5 MKCl. The potential was chosen to exclude all electroactivity and to ensure that the lipid membrane was stable. Further details on the system and how to prepare it are given in [45, 46]. In all cases the data were transformed to the complex capacitance plane and in the first two examples two data matrices were prepared: a 16×50 and a 38×50 matrix of complex numbers. The same matrices would become 16×100 and 38×100 if only real numbers were considered in the data analysis.

The magainin example

Measurements were made with three different concentrations of magainin: 0, 10, and 30 μM. SVD was carried out on the raw complex impedance data (16×50). One component explained 99.3% SS. The Argand diagram for the first component score vector showed that the higher concentration was separated from the lower one. Because of replicate noise, the low and zero concentrations could not be separated. The Argand diagram of the complex first loading showed that low frequencies were responsible for the separation, indicating that the interaction of magainin with the monolayer is a slow process. The results for the 16×100 matrix of real data confirmed these findings, but in a less concentrated manner, making the interpretation more awkward, because of the 100 variables in the loadings.

The gramicidin A example

Measurements were made with different concentrations of gramicidin A in two different electrolyte solutions, i.e.: 0.1 MKCl and 0.05 M$Mg(NO_3)_2$. A time component was introduced by leaving some solutions in the cell for a longer time and remeasuring. The gramicidin A concentrations used were 0, 30, 60 and 130 nM. The Argand diagrams for the residuals showed that some structure was left after one component, but that mainly noise was left after two components. The two components explained 81 and 14% of the SS (Eq. 5). The Argand diagrams for the complex scores could be used to explain a difference for the K and Mg solution experiments, a concentration dependency, and a time dependency. Also the spread of replicate measurements was clearly seen. The first component loading showed a semicircle at high frequencies and a tail at low frequencies. The most dominant difference in the spectra with different cations is the size of the high-frequency semicircle. The second component loading indicated that three different types of low-frequency interactions contributed to the separation of the scores from measurements in $Mg(NO_3)_2$ and KCl, respectively.

The bacterial peptide CNY21L example

Impedance was measured for four different concentrations of peptide CNY21L (0.02, 0.08, 0.20, and 0.80 μM) in substrate DOPC. Duplicate measurements were performed for the latter three concentrations, resulting in seven samples in total. Each sample was measured prior to addition of CNY21L and after 1.5, 15, and 30 min. This gave a total of 28 sample measurements. Fifty impedance frequencies, logarithmically distributed between 0.1 and 65 kHz, were recorded for each measurement. The data were transformed to complex capacitance. The replicates were averaged (Fig. 2) and assembled in a matrix with 13 objects and 50 complex variables. The matrix was mean-centered and unit variance scaled. SVD was then calculated, giving one component explaining 96.1% SS. This is an indication that measurement noise is rather low.

The complex score Argand plot including all measurements shows that the concentration dependence is complicated (Fig. 3). This can be linked to the nonlinear behavior that is observed in the low-frequency range in the dielectric loss spectrum (Fig. 2b). This is clear indication that more

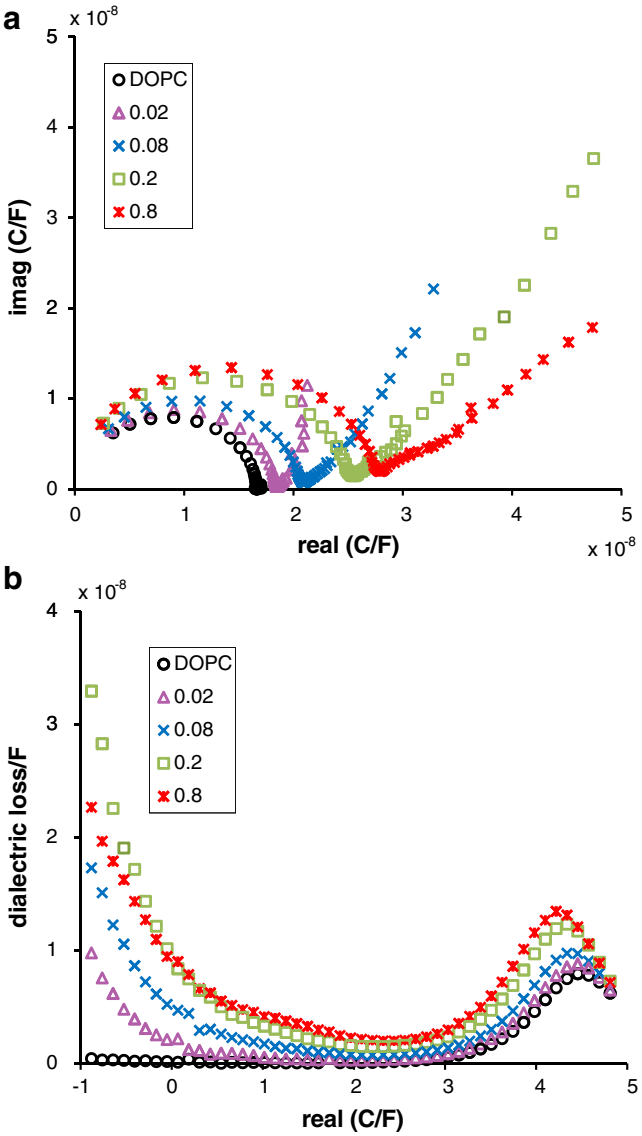

Fig. 2 **a** The averaged raw data as a complex plane plot. **b** Averaged dielectric loss spectra. *DOPC* dioleyl phosphatidylcholine

than one process is occurring that is related to the concentration of the peptide in solution. The time dependence is in a diagonal direction as indicated with an arrow in Fig. 3. For a deeper understanding, the loading plots are shown in Fig. 4.

The real part of the first component does not show much structural detail (Fig. 4b). All frequencies from 0.1 to 10,000 Hz are responsible for a shift in the positive direction along the real *v*(1) axis related to both time and concentration. The shift is due to the continuous increase in the real component owing to interaction of the peptide with the monolayer. This is supported by the original data (Fig. 2a). At higher frequencies above 10,000 Hz, there is a shift from positive to negative loadings.

The imaginary part of the first component has detailed features (Fig. 4c). At high frequencies, i.e., frequencies above 10,000 loadings, large negative values are observed and these are probably related to the time and concentration dependence in the high-frequency dielectric loss peak. The lower the concentration of the peptide, the smaller the time dependence and vice versa. Thus, the final scores, after 30 min, from the two highest concentrations are found in the lower-right corner of the SVD score plot.

At frequencies between 100 and 1,000 Hz the im(v1) loadings are approaching zero. This coincides with an almost invariant imaginary part of the capacitance at all concentrations in this frequency regime.

At frequencies between 10 and 100 Hz there is an increasing negative trend in the im(v1) loadings and this might reflect the observed tendency to a small dielectric loss peak in the capacitance plot at f ≈50 Hz (Fig. 2b). At even lower frequencies, i.e., down to 0.5 Hz, there is a further negative trend in the loadings.

Thus, a broad distribution of interactions is observed between 0.5 and 100 Hz that produce a separation in the plots along the imaginary axis. These are probably related to the concentration of the peptide. The stepwise decrease in im(v1) in this frequency regime indicates there is more than one type of relaxation, which is also supported by the complicated concentration dependence in the score plot. Considering the small data set that is prevalent in this study, it would be far-fetched to draw any conclusions on the origin of these low-frequency relaxations. They might have the same origin but with a broad distribution of relaxation times.

In an earlier work [44], it was shown that the positively charged (III^{+}) antimicrobial peptide CNY21L interacts with a lipid layer in two ways. Firstly, there is an *electrostatic interaction* that is probably related to the observed increase

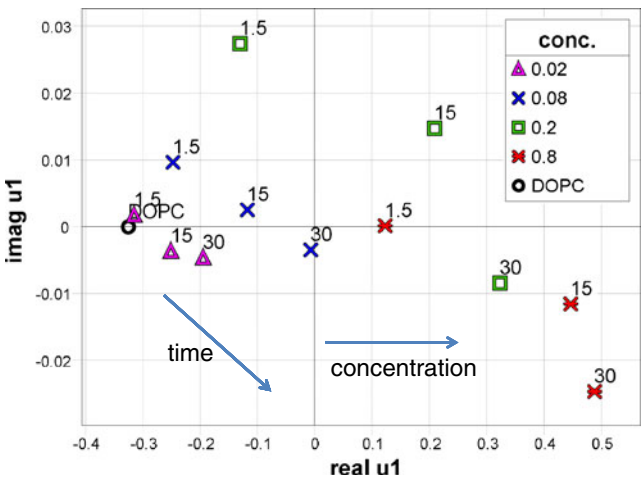

Fig. 3 The first score in the complex plane with time and concentration indicated. The numbers *1.5*, *15*, and *30* represent the exposure time in minutes after addition of peptide

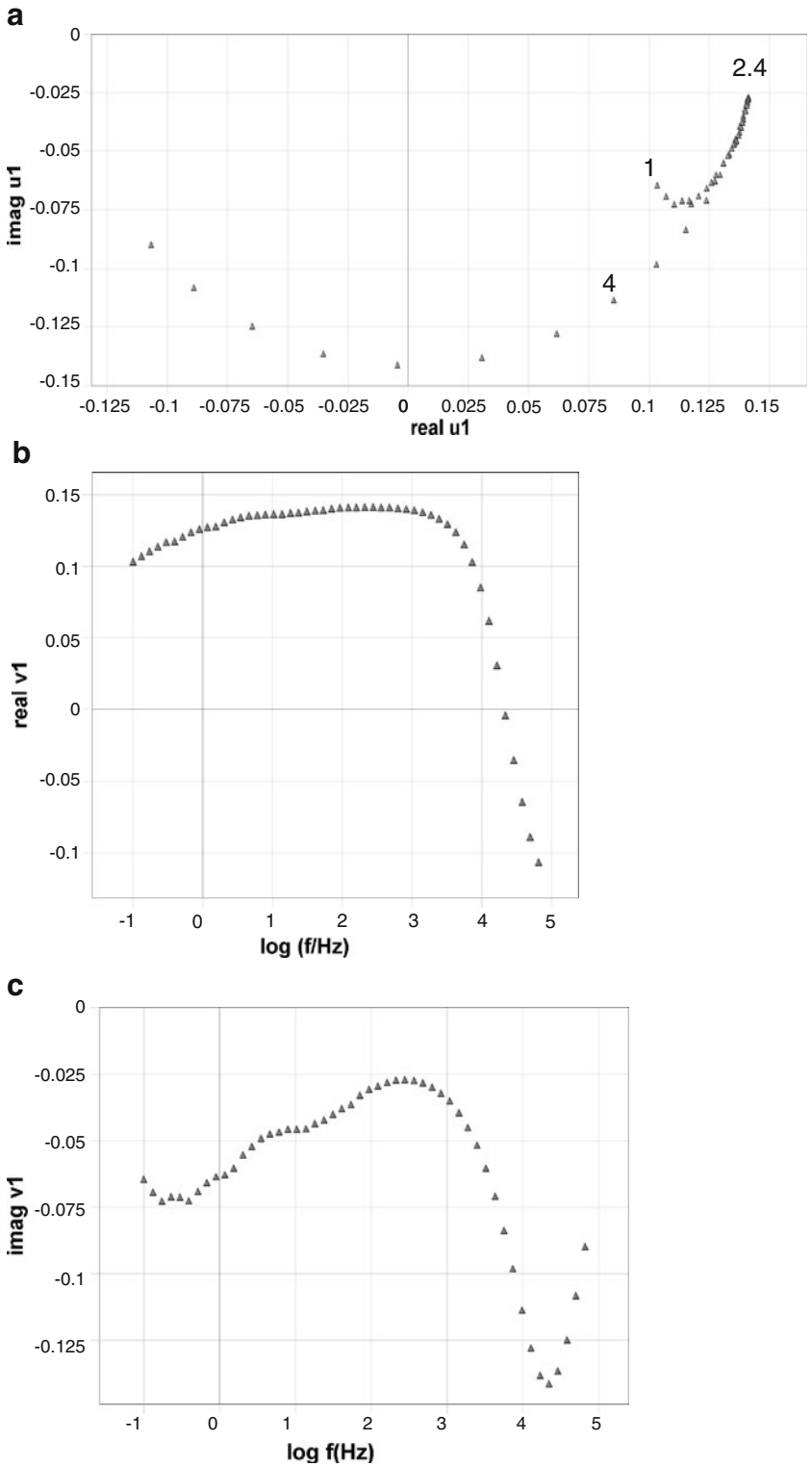

Fig. 4 **a** The first loading in the complex plane. **b** The real value of the first loading against the logarithm of frequency. **c** The imaginary value of the first loading against the logarithm of frequency

in high-frequency capacitance. The peptide is known to penetrate deeply into the lipid membrane and therefore we suggest that the low-frequency contribution is related to *hydrophobic interaction* and a slow rotation of the peptide in the monolayer.

Future aspects

Impedimetric biosensors have great potential in future online monitoring in, for instance, environmental control or bedside diagnostics. The various methods for analysis of

the impedance data were discussed earlier. The faradaic sensor systems are very sensitive but unfortunately there use is time consuming and they are not suitable for online monitoring. The nonfaradaic sensor systems are often simplified and there is some likelihood that subtle interactions are discarded in the equivalent circuit that is employed.

In the present paper, we argued that multivariate analysis of impedance data is a most suitable method for two reasons: (1) the possibility to detect unknown weak interactions in the low-frequency regime is recognized since the major part of the α dispersion due to tangential diffusion is excluded; (2) these specific interactions might contribute to very low detection limits in analytical applications with multivariate regression.

In this paper, one aspect from impedance measurements on the microbial peptide was discussed for didactic reasons. A more thorough interpretation of all facets of the available data will be presented elsewhere.

The following two important citations from MacDonald [47] reflecting on the history of electrochemical impedance spectroscopy are worth considering:

1. ...interpretation of EIS data is basically a "pattern recognition" problem, in which a mechanism or analog is sought that reproduces the loci of the experimental data as a function of all accessible independent variables using a single set of model parameters, as determined by optimisation of the model on the experimental data. Noting that all experimental data are inaccurate, to one extent or another and that models are only our perceptions of reality and hence are incomplete, the model does not exist and indeed many models may be found to represent the experimental observations equally well.
2. Thus the challenge of the future is to devise methods for differentiating between candidate mechanisms that differ only in ever increasingly subtle detail.

We agree with MacDonald and suggest that the method presented in this paper has the potential to provide a tool that will help to find the correct model and to find subtle and to date unknown details in the impedance spectra.

Acknowledgement The European Union Structure Foundation Objective 2 is recognized for its financial support.

References

1. Forster RJ (1996) Analyst 121:733–741
2. Wang J (2006) Biosens Bioelectron 21:1887–1892
3. Rasooly A (2006) Biosens Bioelectron 21:1847–1850
4. Rasooly A, Jacobson J (2006) Biosens Bioelectron 21:1851–1858
5. Pravda M, Kreuzer MP, Guilbault G (2002) Anal Lett 35:1–15
6. Sapsford KE, Charles PT, Patterson CH, Ligler FS (2002) Anal Chem 74:1061–1068
7. Luppa PB, Sokoll LJ, Chan DW (2001) Clin Chim Acta 314:1–26
8. Long YT, Li CZ, Kraatz HB, Lee JS (2003) Biophys J 84:3218–3225
9. Swietlow A, Skoog M, Johansson G (1992) Electroanalysis 4:921–928
10. Whitehouse C, O'Flanagan R, Lindholm-Sethson B, Movaghar B, Nelson A (2004) Langmuir 20:136–144
11. Newman JD, Turner APF (2005) Biosens Bioelectron 20:2435–2453
12. Eldefrawi ME et al (1988) Anal Lett 21:1665–1680
13. Daniels JS, Pourmand N (2007) Electroanalysis 19:1239–1257
14. Katz E, Willner I (2003) Electroanalysis 15:913–947
15. van Gerwen P et al (1998) Sens Actuators B 49:73–80
16. Laureyn W et al (2000) Sens Actuators B 68:360–370
17. Rickert J, Göpel W, Beck W, Jung G, Heiduschka P (1996) Biosens Bioelectron 11:757–768
18. Blonder R, Katz E, Cohen Y, Itzhak N, Riklin A, Willner I (1996) Anal Chem 68:3151–3157
19. Thoelena R et al (2008) Biosens Bioelectron 23:913–918
20. Wang J, Cai XH, Rivas G, Shiraishi H, Farias PAM, Dontha N (1996) Anal Chem 68:2629–2634
21. Patolsky F, Katz E, Bardea A, Willner I (1999) Langmuir 15:3703–3706
22. Patolsky P, Lichtenstein A, Moshe Kotler M, Willner I (2001) Angew Chem Int Ed 40:2261–2265
23. Robertson DL, Joyce GF (1990) Nature 344:467–468
24. Tuerk C, Gold L (1990) Science 249:505–510
25. Ellington AD, Szostak JW (1990) Nature 246:818–822
26. Wang J, Meng WY, Zheng XF, Liu SL, Li GX (2009) Biosens Bioelectron 24:1598–1602
27. Polsky R, Gill R, Kaganovsky L, Willner I (2006) Anal Chem 78:2268–2271
28. Sharon E, Freeman R, Tel-Vered R, Willner I (2009) Electroanalysis 21:1291–1296
29. Liao W, Cui XT (2007) Biosens Bioelectron 23:218–224
30. Miura Y, Kimura S, Kobayashi S, Imanishi Y, Umemura J (2000) Biopolymers 55:391–398
31. Lindholm-Sethson B, Geladi P, Nelson A (2001) Anal Chim Acta 446:121–130
32. Varshney M, Li Y (2009) Biosens Bioelectron 24:2951–2960
33. Foster KR, Schwan HP (1989) Crit Rev Biomed Eng 17:25–104
34. Kell DB, Davey CL (1990) In: Cass AEG (ed) Conductimetric and impedimetric devices in biosensors, a practical approach. IRL Press, Oxford University, pp 125–154
35. Fricke H (1925) J Gen Physiol 9:137–152
36. Macdonald JR (1987) Impedance spectroscopy; emphasizing solid materials and systems. Wiley, New York, chap 2
37. Grimnes S, Martinsen OG (2000) Bioimpedance&bioelectricity. Academic, London
38. Awayda MS, Van Driessche W, Helman SI (1999) Biophys J 76:219–232
39. Fatt P (1964) Proc R Soc Lond B 159:606–651
40. Falk G, Fatt P (1964) Proc R Soc Lond B 160:69–123
41. O'Brien RW (1982) Adv Colloid Interface Sci 16:281–320
42. Harris CM, Kell DB (1985) Eur Biophys 13:11–24
43. Geladi P, Nelson A, Lindholm-Sethson B (2007) Anal Chim Acta 595:152–159
44. Ringstad L, Protopapa E, Lindholm-Sethson B, Schmidtchen A, Nelson A, Malmsten M (2008) Langmuir 24:208–216
45. Pagano RE, Miller IR (1973) J Colloid Interface Sci 45:126–137
46. Nelson A, Benton A (1986) J Electroanal Chem 202:253–270
47. MacDonald DD (2006) Electrochim Acta 51:1376–1388